Tomography characterization of solid oxide fuel cells using high-energy transmission x-ray microscopy

Chen Zhang[a], P. Kenesei[b], S. D. Shastri[b], and R. M. Suter[a]

[a]Department of Physics, Carnegie Mellon University, Pittsburgh, PA, USA

[b]Advanced Photon Source, Argonne National Laboratory, Argonne, IL, USA

February 26, 2019

1 Motivation

High-energy transmission x-ray microscopy (HETXM) can provide tomography characterization with sub-micron spatial resolution for samples that are too thick for conventional nano-CT characterization [S. D. Shastri, 2015]. In this study, the tip region ($20 \times 20 \times 100\,\mu m$) of a solid oxide fuel cell (SOFC) was characterized using HETXM. The sinograms collected from the HETXM experiment were used to reconstruct the morphology of the tip using open source tomography reconstruction suite TomoPy [Gürsoy et al., 2014], the results of which were used to evaluate the porosity state of the tip of the SOFC.

2 Experiment

The HETXM experiment was performed at the advanced photon source beamline 1-ID in the Argonne national laboratory using the standard HETXM configuration developed by S. D. Shastri [2015]. A total number of six tomography scans were conducted at $\sim$50 keV using a far-field detector (2048×2048 pixel resolution) with a step size of $0.1°$, resulting in an effective detection resolution of $200\,nm$/pixel. Although all six tomography scans covering different regions of the SOFC pillar yielded projection images

suitable for tomography reconstruction, only the tip of the SOFC was reconstructed and analyzed in this study, mostly as a proof of concept.

3 Tomography reconstruction

3.1 Data preprocessing

The reflective lenses and the associated sub-micron resolution of HETXM makes the collected projection images more sensitive to the beam instability (beam wiggling and intensity fluctuation) and dynamic misalignment [1] when compared with conventional high-energy tomography characterization. Therefore, projection images collected from HETXM need to be corrected for both factors prior to tomography reconstruction.

3.1.1 Correction for beam instability

Similar to conventional tomography characterization, the projection images collected from HETXM contains beam characteristics, which can be in theory removed by subtracting the flat field images (Fig. 1) following Beer's law. However, the beam wiggling (spatial instability) and beam intensity fluctuation (temporal instability) can leave residual beam characteristics in the normalized projection images. Consequently, advanced background normalization is necessary to further minimize these residual beam characteristics.

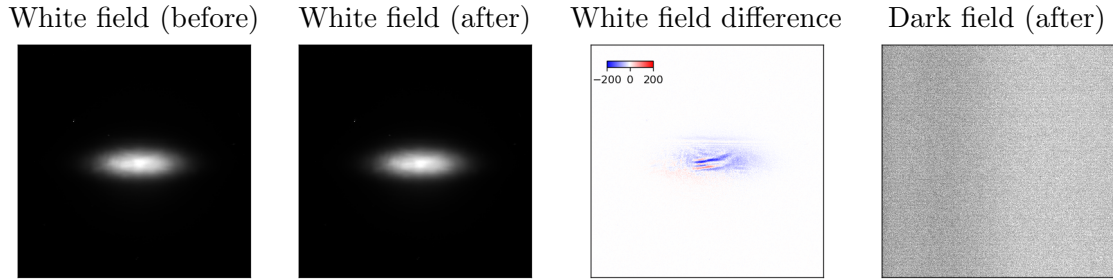White field (before) White field (after) White field difference Dark field (after)

Figure 1: The median of background (white and dark) images collected before and after the tomography scan. The dynamic range of the white field images are $[0, 4000]$ (counts) while the dynamic range of the dark field image is $[0, 10]$ (counts).

Prior to the advanced background normalization, the analysis window is reduced from the detector size (2048×2048) to the sample region (500×400) such that the reduced image stack ($\sim 7\,\mathrm{GB}$) can fit in a modern computer with double precision (64bit float). Given that impulse noise is a common issue in high-energy tomography characterization,

---

[1] The far-field detector can tilt and drift slightly with respect to the beam axis during the experiment, and the associated artifacts can be amplified by the HETXM configuration.

selective median filter [2] was applied to each individual sinogram to reduce the impulse noises (Fig. 2).

For a normalized sinogram from an ideal tomography characterization, the dark region of the sinogram (< 1) denotes the sample attenuation strength whereas the rest (air) should be white ($= 1$). However, the residual beam characteristics due to beam wiggling and intensity fluctuation often leaves horizontal linear features observed in Fig. 2, which can be removed by rescaling each row of the sinogram such that the air region remains one (zero attenuation). In this study, this process is automated with the following algorithm

- Calculate the cumulative intensity profile of each sinogram i using $I_i = \sum_\omega I_i^\omega$.

- Use the second order derivative of I_i to locate the left and right air stripes for each sinogram i.

- For each sinogram i, calculate the average intensity for each row in the left and right air stripes.

- For each sinogram i, rescale the intensity of each row such that the average intensity in the left and right air stripes are one.

- Calculate the total intensity difference ΔI due to the advanced normalization.

- Repeat previous steps until ΔI falls below certain tolerance.

In this study, it was found that a total number of ten iterations [3] of the advanced background normalization can successfully remove the horizontal linear artifacts in each sinogram, regardless of the signal to noise ratios (Figs. 3 to 5). Furthermore, it was found that that beam has minimum wiggling during this HETXM experiment as no obvious gradient can be found in each row of the difference sinogram (the right most sinograms in Figs. 3 to 5).

3.1.2 Correction for dynamic misalignment

In an ideal tomography characterization setting, a single rotation axis is shared by all 180°-pair of projections due to the nature of the experiment. However, dynamic misalignment could occur during the experiment due to the shifting/drifting/vibration of both the detector and sample stage. For conventional high-energy tomography characterization, this effect is often well-below the experiment resolution, rendering its negative impact negligible. This unfortunately does not hold true for HETXM due to its innate high spatial resolution, which often results in the appeared sample jittering in the collected projections.

---

[2] The selective median filter replace the outliers (impulse noises) with the median value calculated within a given kernel.

[3] One might also argue that one iteration is sufficient as ΔI decays rapidly as shown in the left most figures of Figs. 3 to 5
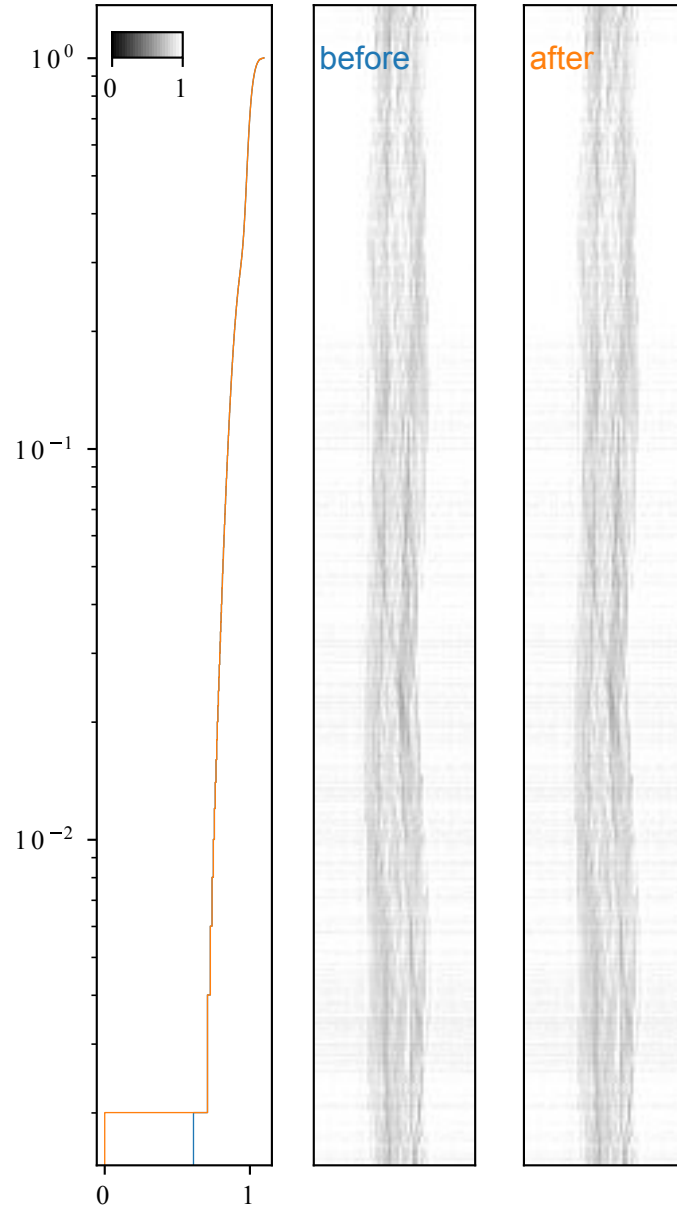
Figure 2: Remove impulse noise from one example sinogram using selective median filter with a 3×3 kernel.
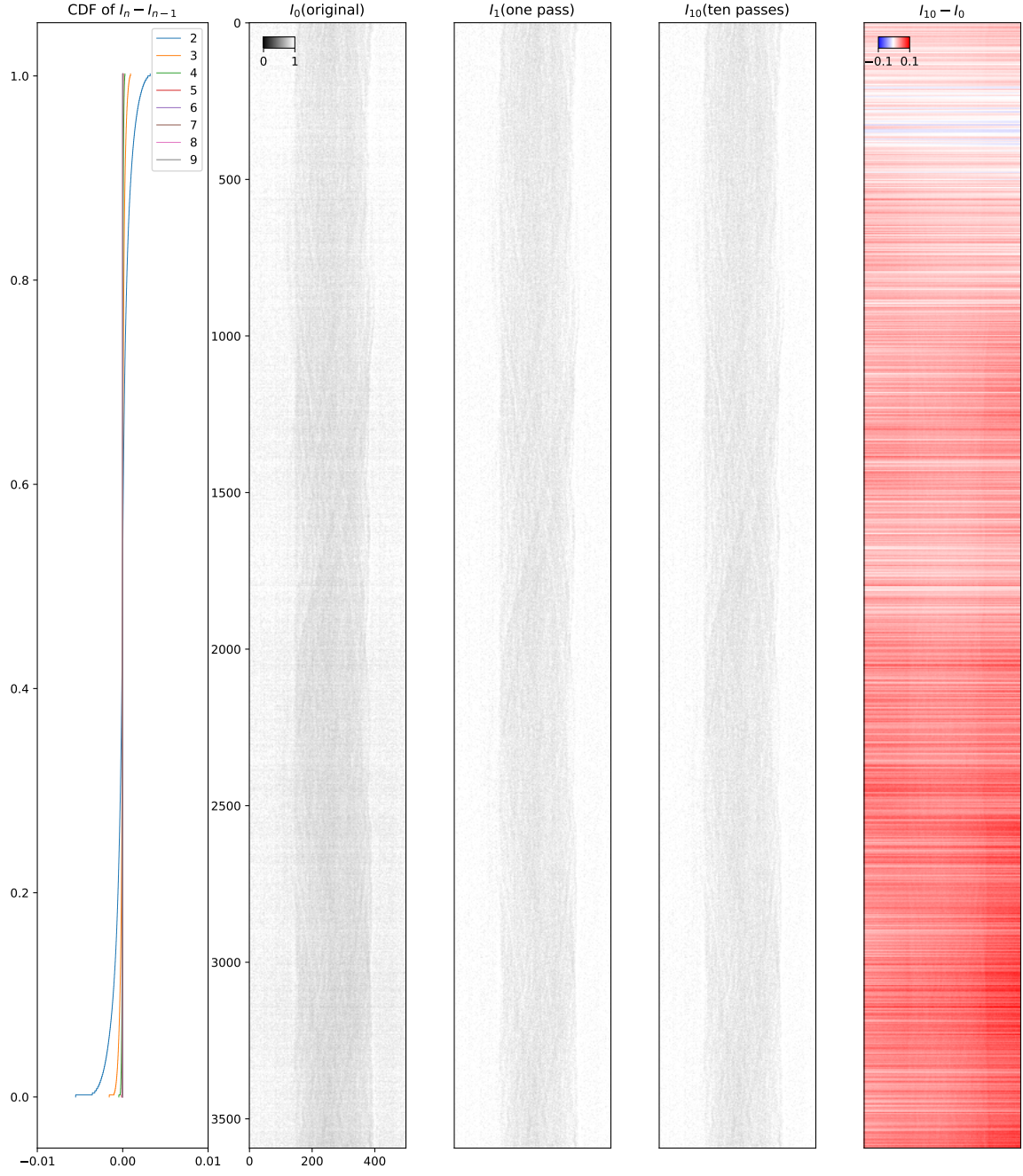
Figure 3: Demonstration of the advanced background normalization in the top region of the projections with relatively **low** signal to noise ratio.
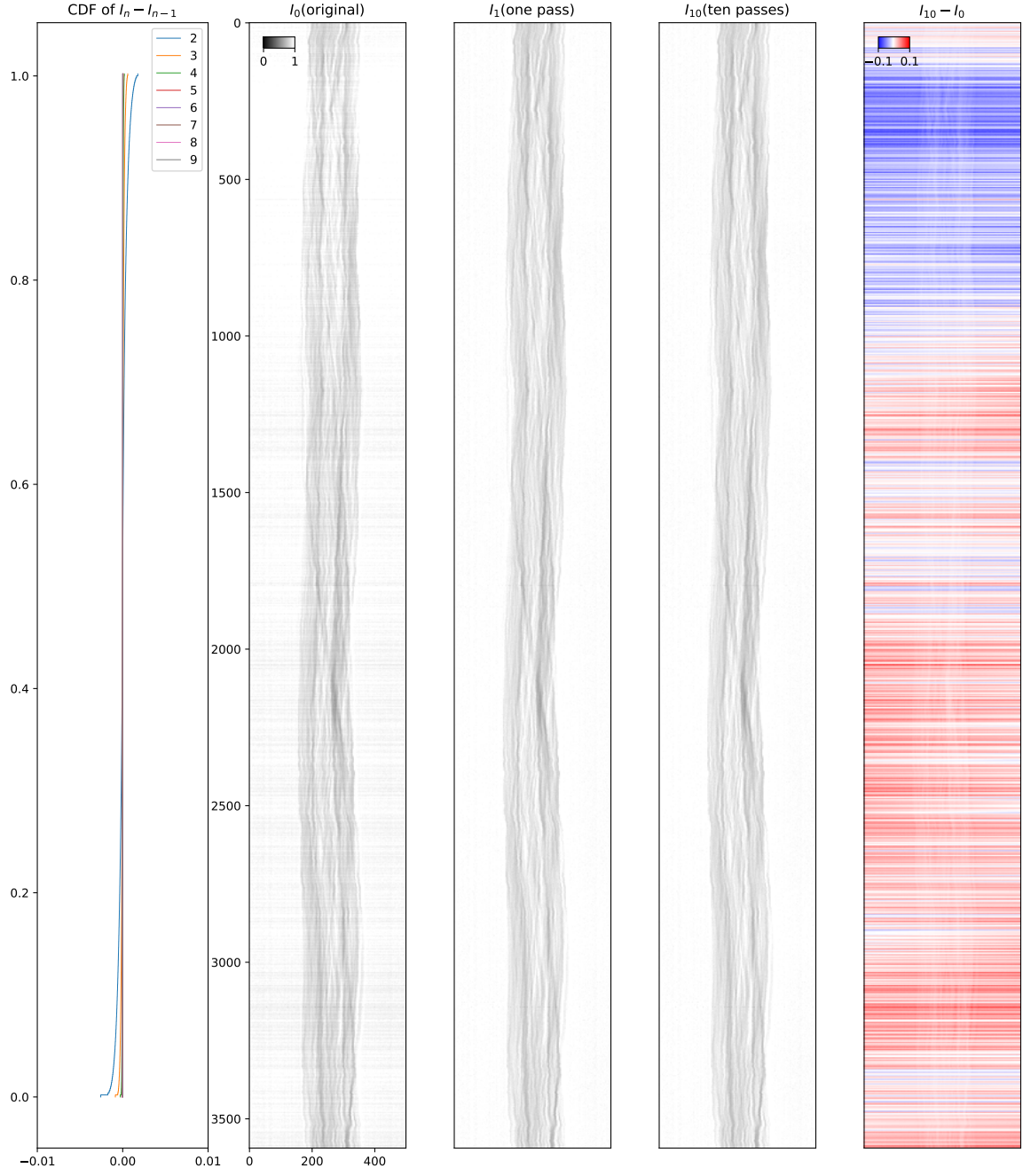
Figure 4: Demonstration of the advanced background normalization in the middle region of the sample with relatively **high** signal to noise ratio.
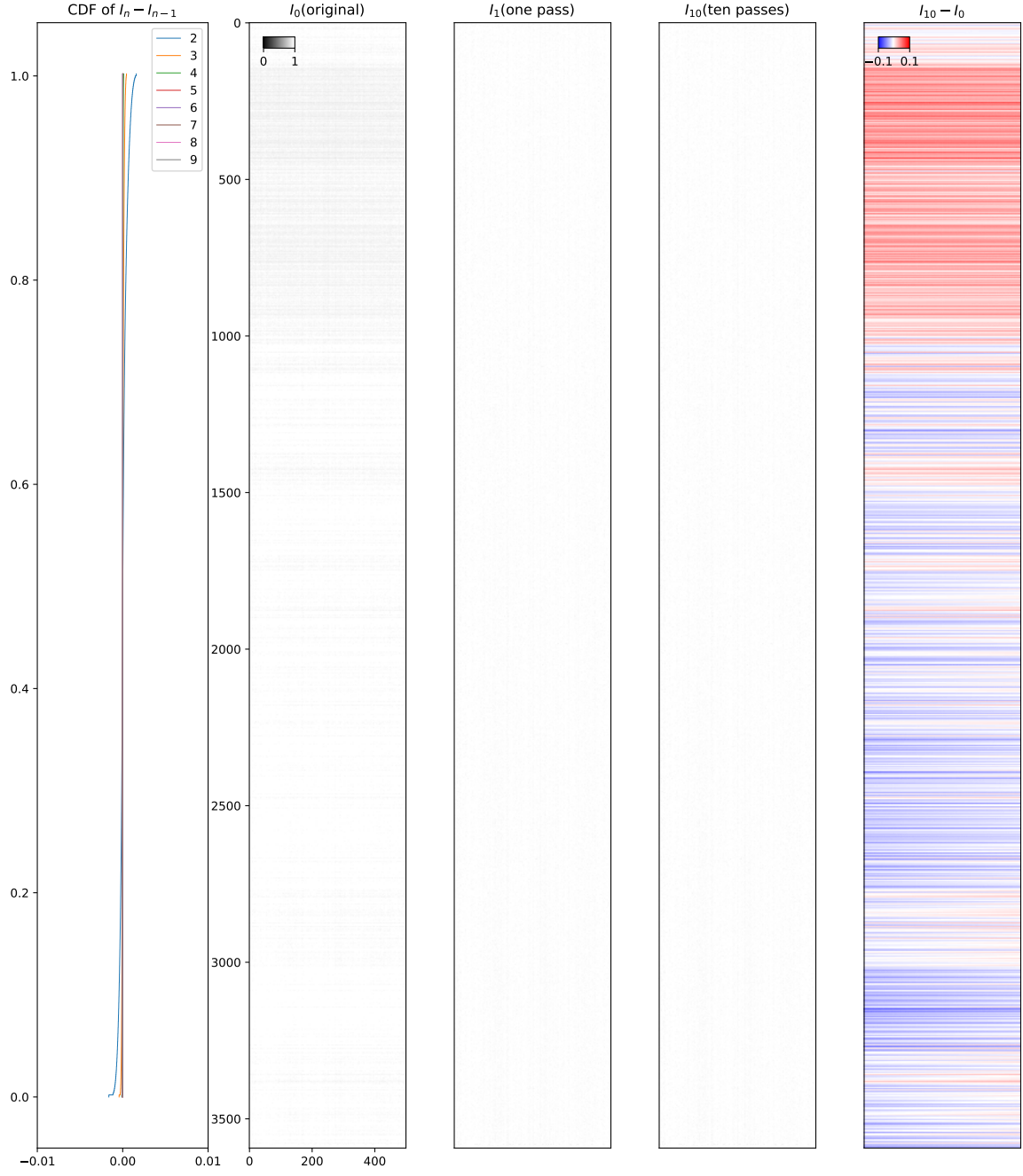
Figure 5: Demonstration of the advanced background normalization in the bottom region of the projections with **no** sample signals.

Using the center column of the projection image as a reference, one could correct the horizontal component of the dynamic misalignment by systematically shifting the rotation axis of 180°-pair projections to the reference rotation axis. In this study, this process was realized as the following steps:

- Calculate the pair-wise rotation center (horizontal component of the rotation axis) of each 180°-pair using a sub-pixel image registration algorithm developed by Guizar-Sicairos et al. [2008].

- Calculate the difference (δ_h) between the pair-wise rotation center and the horizontal center of the projection image (Fig. 6).

- Inspect the pairs with extremely large deviation (outliers), and remove the pairs contain corrupted frames (Fig. 7).

- Shift each 180°-pair of projections such that all projection images share the same rotation axis (the reference rotation axis).
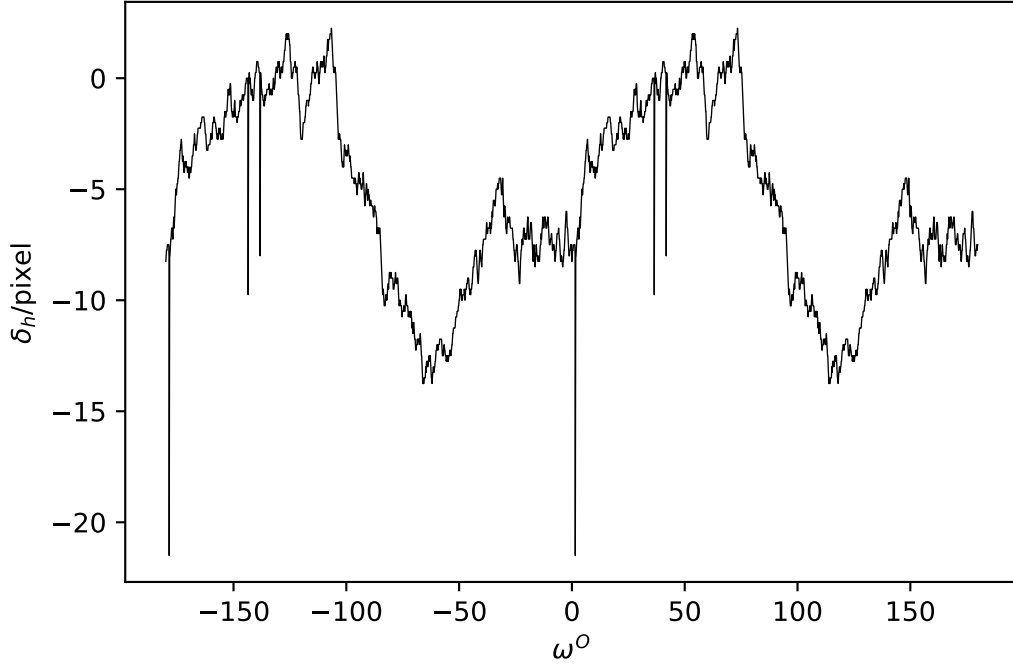

Figure 6: The corrupted frames can be detected by checking the outliers in the profile of 180° pair-wise rotation axis where δ_h denotes the amount of horizontal offset between rotation axis and the image center column.

In theory, one should also correct for the **vertical** component of the dynamic misalignment. However, this was deemed impossible with current HETXM configuration due to *the lack of a common reference point*. Therefore, the vertical component of the dynamic misalignment was left uncorrected in this study.
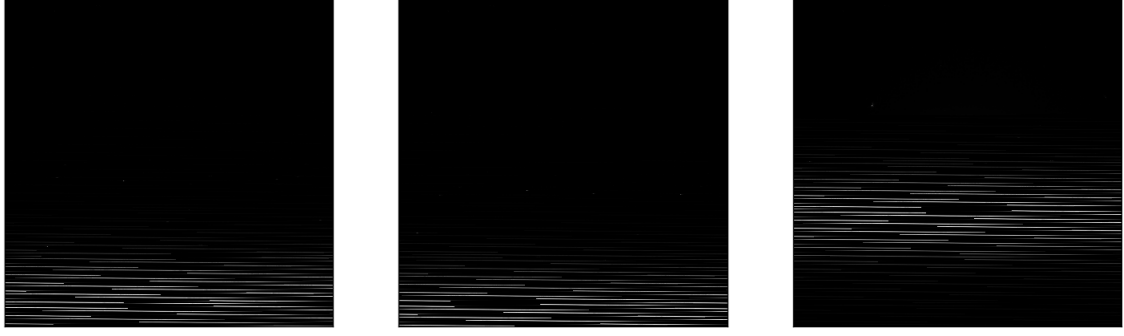
8

Figure 7: Three corrupted frames were detected out of the total 3600 frames. These corrupted frames and the associated 180° pairs were excluded from the tomography reconstruction as it is not possible to adjust a 180° pair horizontally with one corrupted frame.

3.2 Tomography reconstruction

Prior to the actual tomography reconstruction, a per slab based rotation axis deviation analysis was perform for the HETXM data set since a tilted rotation axis is a common problem in standard tomography characterization. More specifically, four 180°-pair of projections were randomly selected from the tomography projection image stacks. Each pair is then vertically divided into 200 slabs with thickness of two pixels. The same image registration based method was used to calculate the rotation axis for each slab in each pair. These per slab based rotation axis centers were then used to calculate the relative deviation (δ_h) with respect to the common reference rotation axis. The general trend of the profile in Fig. 8 (δ_h going from positive to negative when moving from top slabs to lower slabs) indicate that the rotation axis of this HETXM data set is indeed tilted. Therefore, a per slab based tomography reconstruction was performed using the "gridrec" engine and "hann" filter from TomoPy [Gürsoy et al., 2014]. The resulting reconstruction results can be found in Fig. 9.

4 Porosity characterization

The tomography reconstruction results (Fig. 9) demonstrate evident porous characteristics of the tip of the SOFC. In this section, the 2D porosity of the tip of SOFC is systematically characterized using phase retrieval in conjunction with Laplacian of Gaussian (LOG) based blob detection.
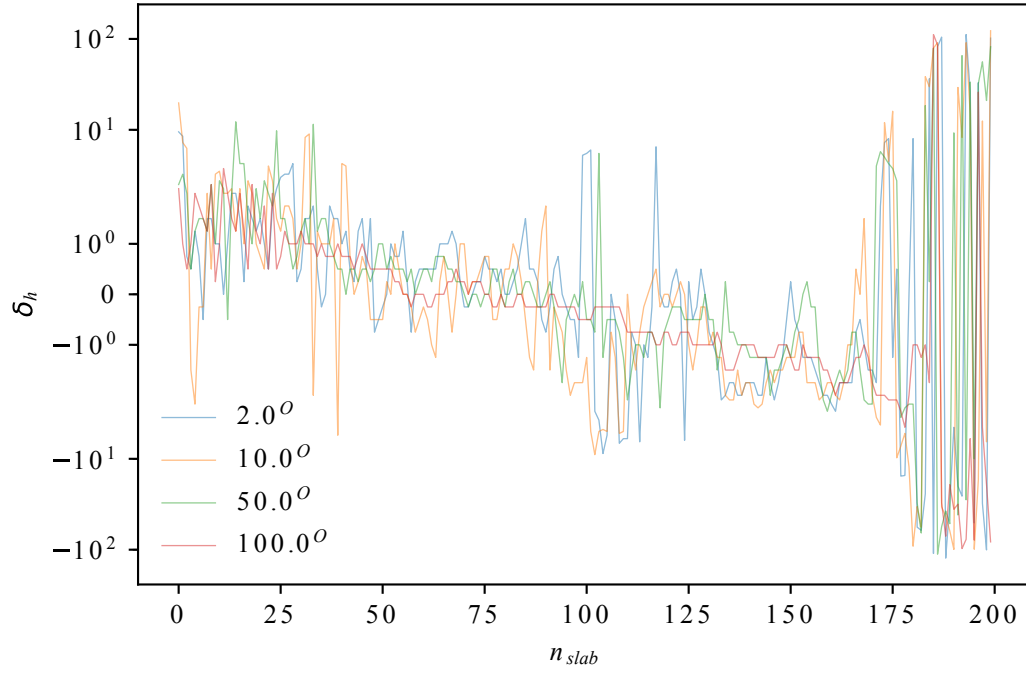
Figure 8: The per slab (2 pixels) based rotation axis deviation profile of four 180°-pair projections indicates that the rotation axis of the collected tomography projection image stack is tilted, which results in the consistent trend going from positive (top) to negative (bottom).
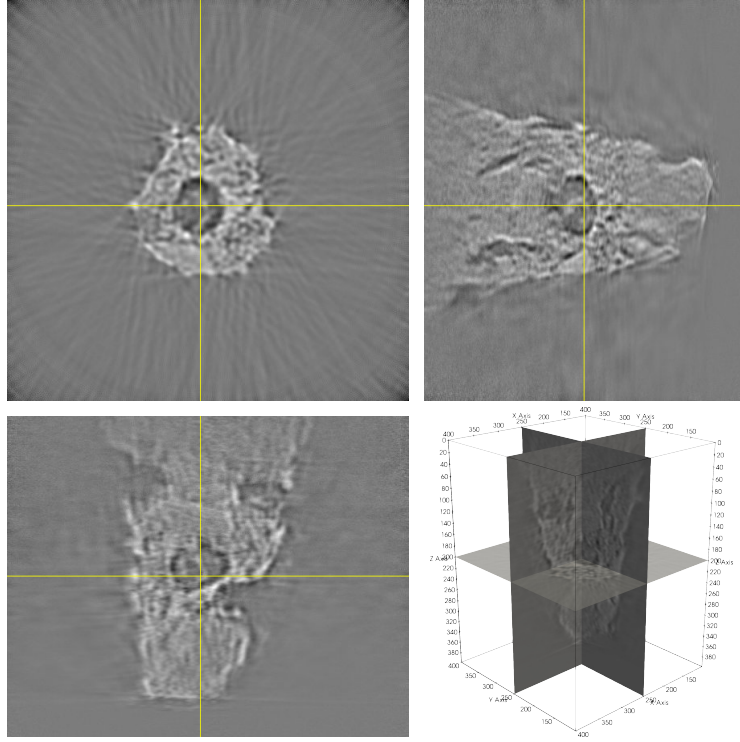
Figure 9: Orthogonal slices of the tomography reconstruction results show evident porous characteristics of the tip of the SOFC.
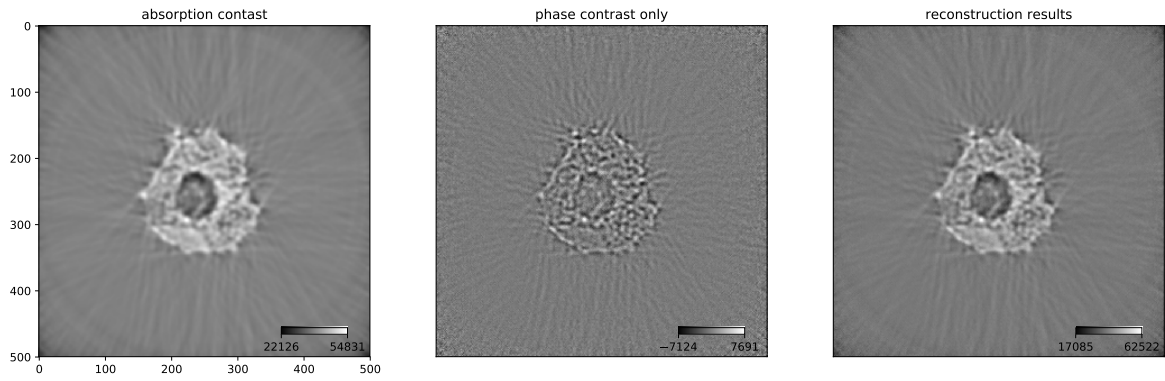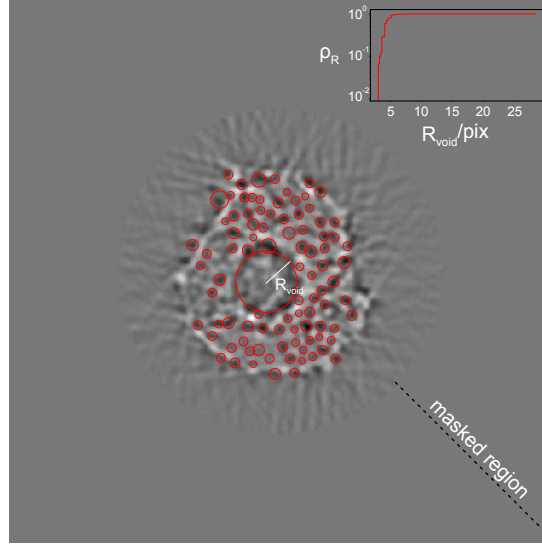

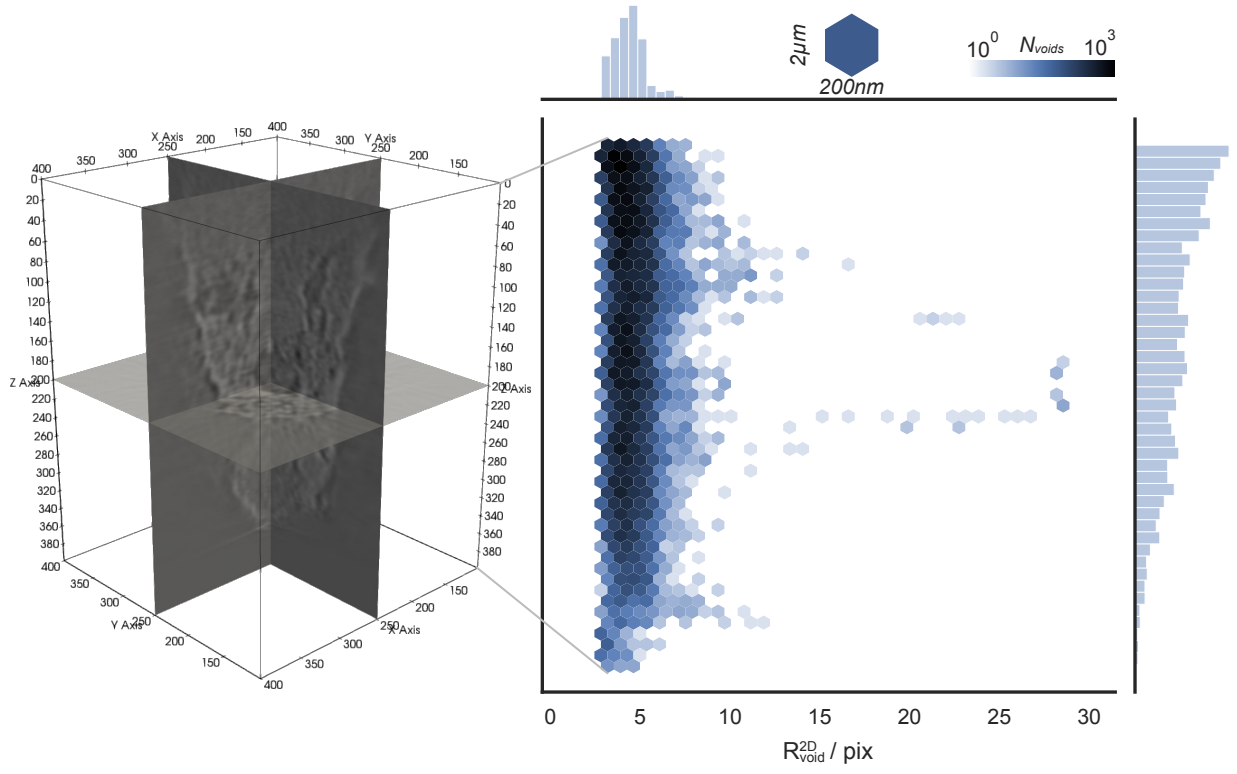Figure 10: phase retrieval demo

Figure 11: void detection demo

Figure 12: void profile

5 Summary

References

Manuel Guizar-Sicairos, Samuel T. Thurman, and James R. Fienup. Efficient subpixel image registration algorithms. *Opt. Lett.*, 33(2):156–158, Jan 2008. doi: 10.1364/OL. 33.000156. URL http://ol.osa.org/abstract.cfm?URI=ol-33-2-156.

Doğa Gürsoy, Francesco De Carlo, Xianghui Xiao, and Chris Jacobsen. TomoPy: a framework for the analysis of synchrotron tomographic data. *Journal of Synchrotron Radiation*, 21(5):1188–1193, Sep 2014. doi: 10.1107/S1600577514013939. URL https://doi.org/10.1107/S1600577514013939.

R. M. Suter S. D. Shastri, P. Kenesei. Refractive lens based full-field x-ray imaging at 45-50 kev with sub-micron resolution, 2015. URL https://doi.org/10.1117/12. 2195531.